The Astronomical Journal, 146:148 (13pp), 2013 December doi:10.1088/0004-6256/146/6/148

THE AGE AND MASS OF THE α HERCULIS TRIPLE-STAR SYSTEM FROM A MESA GRID OF ROTATING STARS WITH $1.3 \leqslant M/M_{\odot} \leqslant 8.0$*

Ehsan Moravveji[1,2,3,4], Edward F. Guinan[3], Habib Khosroshahi[1], and Rick Wasatonic[3]
[1] School of Astronomy, Institute for Research in Fundamental Sciences (IPM), P.O. Box 19395-5531, Tehran, Iran; Ehsan.Moravveji@ster.kuleuven.be
[2] Instituut voor Sterrenkunde, K.U. Leuven, Celestijnenlaan 200D, B-3001, Leuven, Belgium
[3] Department of Astronomy, Villanova University, 800 Lancaster Avenue, Villanova, PA, USA
[4] Department of Physics, Institute for Advanced Studies in Basic Sciences (IASBS), Zanjan 45137-66731, Iran
Received 2013 March 22; accepted 2013 August 29; published 2013 November 1

ABSTRACT

α^1 Her is the second closest asymptotic giant branch (AGB) star to the Sun, and the variable luminous M5 Ib-II member of a triple-stellar system containing G8 III and A9 IV-V components. However, the mass of this important star was previously uncertain, with published values ranging from ∼2–15 $M_{\odot}$. As shown by this study, its fortuitous membership in a nearby resolved triple-star system makes it possible to determine its fundamental properties including its mass and age. We present over 20 years of *VRI* photometry of α^1 Her as well as Wing intermediate-band near-IR TiO and NIR continuum photometry. We introduce a new photometry-based calibration technique and extract the effective temperature and luminosity of α^1 Her, in agreement with recent interferometric measures. We find average values of $T_{\rm eff} = 3280 \pm 87$ K and $\log(L/L_{\odot}) = 3.92 \pm 0.14$. With the MESA code, we calculate a dense grid of evolutionary tracks for Galactic low- to intermediate-mass (1.3 to 8 $M_{\odot}$) rotating stars from the pre-main sequence phase to the advanced AGB phase. We include atomic diffusion and rotation mechanisms to treat the effects of extra elemental mixing. Based on the observed properties of the α Herculis stars, we constrain the age of the system to lie in the range 0.41 to 1.25 Gyr. Thus, the mass of α^1 Her lies in the range $2.175 \leqslant M/M_{\odot} \leqslant 3.250$. We compare our model-based age inference with recent tracks of the Geneva and STAREVOL codes, and show their agreement. In the prescribed mass range for α^1 Her, the observed $^{12}C/^{13}C$ and $^{16}O/^{17}O$ ratios are consistent (within 2σ) with the ratios predicted by the MESA, Geneva, and STAREVOL codes.

Key words: stars: abundances – stars: AGB and post-AGB – stars: evolution – stars: fundamental parameters – stars: individual (alpha[1] Her) – stars: rotation

Online-only material: color figures, supplemental data

1. INTRODUCTION

The details of how a star evolves are mainly governed by three fundamental properties that it inherits from its birthplace: the chemical composition, angular momentum, and mass. The metal content and the projected rotation velocity of a star can be measured from spectroscopy. The mass assessments, however, are currently possible from either asteroseismic analyses of radially and/or non-radially pulsating stars, or more directly from the analyses of the light and radial-velocity curves of double-line spectroscopic eclipsing binary systems. When the seismic and binary information are absent, one classically calculates a grid of stellar models and tries to fit a range of tracks to the observed global properties of the star, such as effective temperature, surface gravity, and luminosity, to estimate other physical properties like age, mass, and radius. However, this grid-based (isochronal) approach has large uncertainties associated with it (Basu et al. 2012); small uncertainties in $T_{\rm eff}$, Fe/H, and $L/L_{\odot}$ translate into large uncertainties in the age and mass of the stars.

In the present study, we pursue the grid-based approach and establish the range of possible masses for the three stars (with a single age) in the α Herculis triple-star system. Our rationale is to take advantage of the fortuitous membership of the bright M5 Ib-II asymptotic giant branch (AGB) star in a resolved triple-star system with a good parallax to determine its physical properties by simultaneously fitting the observed properties. The recent release of stellar evolutionary tracks (mainly by the Geneva group) provides an excellent opportunity to test the model dependence of the inferred physical properties of α^1 Her. For this purpose, we compare MESA with the rotating and non-rotating tracks of Ekström et al. (2012, hereafter E12), Lagarde et al. (2012, hereafter L12), and Mowlavi et al. (2012, hereafter M12).

The stellar mass has an additional critical role: The surface abundances of AGBs depend on the efficiency of the previous dredge-up episodes in addition to (extra) non-convective mixing mechanisms (e.g., Karakas et al. 2010; Abia et al. 2012). Different proposed extra mixing mechanisms are rotation and atomic diffusion (Maeder & Meynet 2012), internal gravity waves (Talon & Charbonnel 2005), magnetic dynamo (Busso et al. 2007), and thermohaline mixing after the sub-giant phase (Charbonnel & Zahn 2007; Cantiello & Langer 2010). The latter affects low-mass stars (Stancliffe 2010), so the net strength of surface enrichments depends explicitly on stellar mass. Since α^1 Her has had its $^{12}C/^{13}C$ and $^{16}O/^{17}O$ isotope ratios measured, here we provide a rare calibration point for these ratios at an intermediate mass and luminosity on the AGB (El Eid 1994).

2. LITERATURE DEBATES ON THE MASS OF α^1 HER

Historically, the reports on the mass of α^1 Her from the literature are inconsistent. They are $M = 15\,M_{\odot}$ by Deutsch (1956), ∼2.0 $M_{\odot}$ by Woolf (1963), 1.7 $M_{\odot}$ by Reimers (1977) and Thiering & Reimers (1993), ∼5 to 7 $M_{\odot}$ by Harris & Lambert (1984) and El Eid (1994), and $2.5^{+1.6}_{-1.1}$ $M_{\odot}$ by Moravveji et al. (2011). This uncertain mass of α^1 Her translates into its

* The grid is publicly available for retrieval.

unknown evolutionary status: assuming a high mass, it could be a red supergiant or a super-AGB star and a progenitor of iron or electron-capture core-collapse supernova (Poelarends et al. 2008; Smartt 2009), while in the lower-mass regime ($M < 5\,M_{\odot}$), the star would be located near the upper tip of the AGB.

The membership of a bright AGB star in a nearby multiple-star system is an excellent opportunity to determine the mass and evolutionary properties of the AGB star. Very few AGB stars have reliable ages and masses. We previously studied the α^1 Her light curve in Moravveji et al. (2010), and extracted the dominant pulsation periods. The purpose of this second paper is to constrain the parameter space of the global physical properties of α^1 Her—i.e., its mass, effective temperature, and luminosity—for a subsequent asteroseismic modeling.

First, we introduce the α Herculis system in Section 3 and our photometric compilation in Section 4. In Section 5 we calibrate the effective temperature based on the strength of the TiO λ7190 absorption bands. In Section 6 we derive the time-variable luminosity and radius of α^1 Her. Based on these, we set up a dense grid of evolutionary models (Section 7). In Section 8, we establish the most likely range for the age of the system and masses of its individual members, and compare our findings with those from three other codes. As a by-product of the grid calculation, we additionally present the explicit dependence of mixing of C and O isotopic ratios on the stellar mass during the AGB phase. We discuss our results in Section 9.

3. THE α HERCULIS SYSTEM

α Herculis is an extensively studied system, and is composed of three stars. Based on the literature, several properties of the system are known to varying accuracies (e.g., Deutsch 1956; Reimers 1977; Thiering & Reimers 1993). McAlister et al. (1989) speculate the presence of the fourth or even fifth members.

The primary, α^1 Her (Rasalgethi; HD 156014, $V = 3.350 \pm 0.003$ mag, $K = -3.511 \pm 0.150$ mag), is an M5 Ib-II (Deutsch 1956; Keenan & McNeil 1989) semi-regularly pulsating bright giant. According to the Morgan & Keenan (1973) classification, the spectra of α^1 Her are a standard for its subclass. The secondary, α^2 Her (HD 156015, $V = 5.39$), is a spectroscopic binary itself (Thiering & Reimers 1993), consisting of a G5 III giant (hereafter α^2 Her A) and an A9 IV-V dwarf (hereafter α^2 Her B). The primary and the secondary are $4\farcs7$ distant (Jeffers & Vasilevskis 1978), so our photometry of the system (Section 4) includes the flux from three members. Where necessary, we have replaced the first *Hipparcos* parallax of Perryman et al. (1997; $\pi = 8.53 \pm 2.80$ mas) with the revised value of van Leeuwen (2007); thus, the distance to the system is

$$\pi = 9.07 \pm 1.32 \text{ mas} \Rightarrow d_{\rm Hip} = 110 \pm 16 \text{ pc}. \quad (1)$$

With the parallax π and the disk limb-darkened angular diameter ϕ expressed in milliarcseconds (mas), the radius of the star can be assessed by

$$R = 107.55 \frac{\phi}{\pi} R_{\odot}. \quad (2)$$

The limb-darkened angular diameter of α^1 Her is already measured by different interferometry groups. Figure 1 in Perrin et al. (2004) addresses the strong wavelength dependence of the angular diameter measurement, from near- to mid-IR (Weiner et al. 2003). The average of the limb-darkened K-band interferometry of Perrin et al. (2004)—from 1996 to 1997—is $\phi = 31.51 \pm 0.08$ mas. A similar assessment by Richichi & Percheron (2002) yields $\phi = 37.22 \pm 2.94$ mas, and Weiner et al. (2003) give $\phi = 39.32 \pm 1.04$. The Benson et al. (1991) measurement gives an almost consistent limb-darkened angular diameter $\phi = 33.0 \pm 0.8$ mas (similar to Dyck et al. 1996). Adopting the near-IR limb-darkened angular diameter measure of Perrin et al. (2004), the interferometric radius of α^1 Her is

$$R_{\rm inter} = 400 \pm 61\, R_{\odot}. \quad (3)$$

The large error in the radius is dominated by the parallax uncertainty. Also, as shown in this study, the diameter of α^1 Her varies by up to $\sim$14%. Additionally, Perrin et al. (2004) find $T_{\rm eff} = 3285 \pm 89$ K. Correcting for the revised 2007 *Hipparcos* parallax, we estimate the luminosity of α^1 Her as $\log(L/L_{\odot}) = 4.25 \pm 0.30$.[5]

Spectroscopic study by Deutsch (1956) indicates that the α Herculis system is enshrouded in an envelope of dust. This was later confirmed by the observations of Thiering & Reimers (1993), who found that the extent of the envelope is larger than the semimajor axis of the visual binary orbit. Recently, interferometric observations by Tatebe et al. (2007) at $\lambda_0 = 11.5\,\mu$m over the period 1989–2004 show evidence that α^1 Her may have experienced a major outburst during 1990 in which $\sim 10^{-6}\,M_{\odot}$ was ejected into the ISM with an approximate ejecta speed of 75 km s^{-1}. The same study finds that the shell has a temperature of 518 K and inner and outer angular radii of 250 and 350 mas, respectively. The mass-loss rate of α^1 Her is $\dot{m} = 1.1 - 1.5 \times 10^{-7}\,M_{\odot}$ yr^{-1} (Reimers 1977; Thiering & Reimers 1993).

Table 1 summarizes a collection of physical parameters of α Herculis stars. They are relevant to our study, and are collected from the literature. Where necessary, we have corrected the first *Hipparcos* parallax of Perryman et al. (1997; $\pi = 8.53 \pm 2.80$) with the revised value of van Leeuwen (2007).

For α^1 Her, the spectroscopic measurements of the surface yields of CNO-processed elements date back to the studies of Thompson & Johnson (1974) and Harris & Lambert (1984). These observational evidences—when directly compared to the theoretical model yields—help gauge the role of different types of composition mixing (e.g., El Eid 1994; Cantiello & Langer 2010). We adopt ^{12}C/^{13}C $= 17 \pm 4$, ^{16}O/^{17}O $= 180^{+70}_{-50}$, and ^{16}O/^{18}O $= 550^{+225}_{-175}$ from Harris & Lambert (1984).

4. MULTI-COLOR PHOTOMETRIC OBSERVATIONS

The photometric data for the α Her system were obtained over more than two decades, and the data are compilations of observations from two different sites. The photometry was conducted with the broadband Johnson V filters and three intermediate-band Wing ABC filters (Wing 1992) at Villanova University (VU) by two 20 and 28 cm Schmidt Cassegrain telescopes. The broadband Johnson *VRI* photometry was obtained using the Fairborn-10 (T2) Automatic Photometric Telescope (APT; Henry & Eaton 1995) at Tennessee State University (TSU). The starting and ending observation dates for each data set are different. The sampling is not regular and depends on the visibility of the star and the weather conditions. The TSU observations commenced in 1986 March, and were discontinued in 2001 June. The TSU photometry was first published in Percy et al. (2001).

[5] Using Equation (3) and the Stefan–Boltzmann law, $\log(L_{\rm new}/L_{\rm old}) = 2\log(R_{\rm new}/R_{\rm old}) = 2\log(d_{\rm new}/d_{\rm old}) \approx -0.05$ dex.

Table 1
Compilation of the Observed Physical Properties of Stars in the α Her System from the Literature

	α^1 Her			α^2 Her A			α^2 Her B		
	Value	Ref.	Note	Value	Ref.	Note	Value	Ref.	Note
Spectral Class	M5 Ib-II	(a, c)	(1)	G8 III	(d)		A9 IV-V	(d)	
$T_{\rm eff}$ (K)	3271 ± 46	(g)	(2)	4900 ± 150	(d)	(3, 4)	7350 ± 150	(d)	
	3285 ± 89	(h)							
	3260 ± 40	(i)	(5)						
$\log(L/L_\odot)$	4.25 ± 0.30	(h)							
	3.68	(d)	(3)	2.10 ± 0.04	(d)	(3, 6)	1.41	(d)	(3)
V (mag)	$+3.350 \pm 0.003$	(c)		+5.6	(a)		+6.6	(f)	
ϕ (mas)	33.0 ± 0.8	(g, i)	(5)						
	31.51 ± 0.08	(h)	(7)						
	39.32 ± 1.04	(j)	(8)						
	37.22 ± 2.94	(k)							
$d_{\rm Hip}$ (pc)	110 ± 16	(l)							
$\dot{M}$ ($M_\odot$ yr^{-1})	1.1–1.5×10^{-7}	(d, e)							

Notes. For the results of this study, refer to Table 4. (1) From Coudé Spectroscopy of Deutsch (1956). (2) See Figure 2, Table 4, and Section 6. (3) We take the mean $L/L_\odot = 10.5 \pm 4.5$ from Thiering & Reimers (1993) and correct for the underestimated distance (70 pc). (4) An error of ± 150 K in temperature for α^2 Her A is assumed. (5) K-band interferometry ($\lambda_0 = 2.2\,\mu$m, $\Delta\lambda = 0.4\,\mu$m). (6) An assumed error of 0.1 mag in m_V translates to an error of $\pm 12\,L_\odot$. (7) Corrected to the revised *Hipparcos* distance, K-band interferometry. (8) Interferometry in mid-infrared ($\lambda_0 = 9.5$ to 11.5 μm). The mid-infrared diameter of AGBs is up to $\sim$30% larger than their corresponding near-infrared diameter.

References. (a) Deutsch 1956; (b) Keenan & McNeil 1989; (c) This study; (d) Thiering & Reimers 1993; (e) Reimers 1977; (f) Woolf 1963; (g) Dyck et al. 1996; (h) Perrin et al. 2004; (i) Benson et al. 1991; (j) Weiner et al. 2003; (k) Richichi & Percheron 2002; (l) van Leeuwen 2007.

Table 2
Photometry of the α Her System in Different Filters in Increasing Central Wavelength λ_0 Order

Filter	Wavelength λ_0 (FWHM) (Å)	Observation Site	Max; Min (mag)	Std. Error σ (mag)	$T_{\rm start}$; $T_{\rm end}$ (MJD)	$1/\Delta T$ (10^{-4} days^{-1})	N
Johnson V	5500 (700)	VU	+2.768; +3.624	0.003	49043; 55076	1.657	728
Johnson V	5500 (700)	TSU	+2.922; +3.792	0.004	46510; 52089	1.792	1766
Johnson R	6400 (1400)	TSU	−2.993; −2.437	0.002	46510; 52089	1.792	1757
Wing-A (TiO)	7190 (110)	VU	+0.093; +0.817	0.005	50489; 55076	1.657	547
Wing-B	7540 (110)	VU	−1.519; −1.012	0.003	50489; 55076	1.657	547
Johnson I	8800 (1500)	TSU	−3.748; −3.455	0.001	46510; 51993	1.823	1697
Wing-C	10400 (420)	VU	−1.707; −1.449	0.002	50489; 55076	1.657	547

For the details of our data set and the observation time baseline, see Table 2. In this table, the first column gives the designations for the filters. The second column gives the central passband wavelength λ_0 accompanied with its corresponding FWHM. The third column shows the observation site. The fourth column gives the maximum and minimum of the magnitude in the corresponding filter for the entire observation due to stellar variability. Note that the variability at shorter wavelengths has larger amplitudes. The fifth column is the standard error. The sixth column gives the start and end dates for the observations at the corresponding site, $T_{\rm start}$ and $T_{\rm end}$, respectively. They are expressed in modified Julian date, MJD = HJD − 2,400,000. The seventh column gives the Rayleigh limit $1/\Delta T$ in units of 10^{-4} days^{-1}, where T is the observation time baseline in days. The last column gives the number of observations taken over the prescribed duration per each site. This photometry includes all three components in the measure but the brightness is dominated by the bright, luminous M5 Ib-II star.

Both the VU and TSU observations were conducted *differentially* with respect to comparison stars. The offset was removed by finding the shift between the two data sets that minimizes the standard deviation of the combined data set during the observed overlapping runs. The compiled light curves in the Johnson V and Wing ABC filters are shown in Appendix A (Figure 11). Note that, from shorter to longer wavelengths, the star appears brighter (see Benson et al. 1991 and the fourth column in Table 2), and the amplitude of light variability decreases. This is similar to the pulsation behavior of Mira-type stars (e.g., Lockwood & Wing 1971).

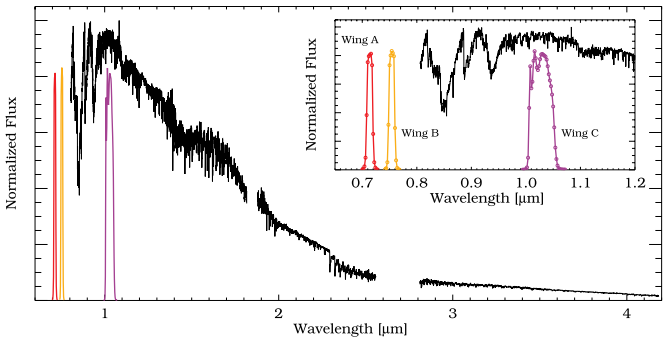

Figure 1. Near-IR spectra of α Her taken from Rayner et al. (2009). The transmission functions for Wing ABC filters are plotted. The Wing C filter sees through the peak of the continuum.

(A color version of this figure is available in the online journal.)

Figure 1 presents the low-resolution spectra of α Her published by Rayner et al. (2009). It covers the wavelength range of 0.8 to 4.2 micron. The Wing ABC transmission functions S_λ are also plotted. These three filters were selected by R. Wing (2010, private communication) for measuring the temperatures and luminosities of evolved M-type stars. The TiO (γ, 0, 0)

λ7190 absorption band strength is very sensitive to the temperature for evolved M stars. The A filter with $\lambda_0 = 7190$ Å is centered on the TiO band, and serves as a reference measure of the TiO band strength. The B filter at $\lambda_0 = 7540$ Å is located essentially on the continuum region. The measured flux in the C filter at $\lambda_0 = 10400$ Å can be corrected to give the bolometric magnitude $m_{\rm bol}$ and luminosity L (Section 6). In Appendix B, we show that this bolometric correction to the Wing C filter is in fact $\rm BC_C = 1.735 \pm 0.030$ mag. The main conclusion from Figure 1 is that the Wing C filter does not suffer from strong absorption bands and measures the peak of continuum of an M5 AGB. Compared to the Johnson V bandpass, it also suffers less from strong TiO absorption bands.

5. EFFECTIVE TEMPERATURE CALIBRATION

5.1. Input Standard Stars

Levesque et al. (2005) provide spectrophotometric temperature calibrations for 74 galactic red supergiants based on $(V-K)_0$ colors and synthetic MARCS stellar atmosphere models. For bright M5 AGBs, their Table 5 gives $T_{\rm eff\text{-}M5\,I} = 3450$ K, which does not agree well with the $T_{\rm eff}$ value determined from interferometry (Table 1). However, α^1 Her is the only M5 star in their list, thus the derived $T_{\rm eff}$ and V-filter bolometric correction ($\rm BC_C$) for such late-type stars are large, subject to uncertainties, and are not always reliable. Our independent calibration yields ∼200 K cooler $T_{\rm eff}$ for M5 AGBs.

Eighteen standard stars were selected from Wing (1978) and were repeatedly observed at the VU site through Wing ABC filters. This helps to define two color indices—γ_1 and γ_2—for each of these stars. Following Wing (1992), the $B - C$ color index

$$\gamma_1 = (B - C), \tag{4}$$

in M-type giant stars is sensitive to temperature variations, since it tracks the slope of the tail of Planck distribution. Hence, it can be calibrated to yield the effective temperature of such late-type stars; yet, some absorption bands may interfere. Thus, the other color index, which is called the TiO index γ_2 and defined as

$$\gamma_2 = A - B - 0.13\gamma_1, \tag{5}$$

is less affected by TiO absorption lines and tracks the changes in the temperature better (Wing 1992). The complete list of Wing standard stars, along with their measured mean $\bar{\gamma}_2$, is presented in Table 3, where the first column is the identification number and the second column gives the stars' HR designations. The third column gives the spectral classification taken from Wing (1978). The fourth column gives the effective temperatures taken from Levesque et al. (2005). The last column is the average $\bar{\gamma}_2$ for each of the program stars. Since γ_2 could be time variable for the standard stars as for α^1 Her, we average over their γ_2 values during our long-term monitoring. The list of program stars is sorted by decreasing $T_{\rm eff}$.

Figure 2(a) shows the time variability of γ_2. Due to the observed Long Secondary Period (LSP; Kiss et al. 2006; Percy et al. 2001) of α^1 Her, γ_2 varies with a period of ∼1400 days; this can serve as an evidence for the pulsation origin of the LSP.

5.2. Calibrating $T_{\rm eff}$ versus the γ_2 Color Index

To arrive at a reasonable calibration for $T_{\rm eff}$ versus TiO index γ_2, we use a Levenberg–Marquardt least-squares (Markwardt 2009) third-order polynomial fit to the entries in Table 3, and

Table 3
The List of Standard Stars from Wing (1978)

ID	HR Number	Spectral[a] Class	$T_{\rm eff}$[b] (K)	$\bar{\gamma}_2$[c] (mag)
1	6705	K5.0	3940	0.202
2	248	K5.4	3920	0.222
3	337	M0.5	3934	0.349
4	8284	M1.0	3817	0.400
5	48	M1.5	3778	0.474
6	45	M2.0	3736	0.560
7	750	M2.5	3690	0.627
8	9064	M3.0	3641	0.759
9	9089	M3.4	3599	0.892
10	211	M4.1	3522	1.026
11	4483	M4.5	3475	1.250
12	4909	M5.1	3401	1.424
13	587	M5.1	3401	1.508
14	5512	M5.5	3348	1.576
15	4267	M5.9	3294	1.725
16	7941	M5.9	3294	1.618
17	6146	M6.6	3194	1.694
18	3639	M7.1	3118	1.941

Notes.
[a] The spectral classes are assigned by Wing (1978).
[b] $T_{\rm eff}$ is taken from Levesque et al. (2005) for mid-K to mid-M giants and supergiants.
[c] $\bar{\gamma}_2$ was measured at VU.

derive the best-fit coefficients. The reduced χ^2 goodness of fit is $\chi^2_{\rm red} = 1.02$. Very similarly, γ_1 could also be used, but we prefer γ_2 for its higher sensitivity to temperature changes due to TiO absorption. Therefore, we end up with the following relation:

$$T_{\rm eff} = 4129(\pm5) - 952(\pm20)\,\gamma_2 + 547(\pm22)\,\gamma_2^2 - 168(\pm7)\,\gamma_2^3. \tag{6}$$

Compare this with last equations in Levesque et al. (2005). The numbers in the parentheses are the 1σ uncertainties for each of the fitting coefficients. The resulting fit is shown as a solid line in Figure 3. The average of the TiO index for α^1 Her is $\gamma_2 = 1.683 \pm 0.003$ mag. Consequently, the average effective temperature after substituting mean γ_2 into Equation (6) is $T_{\rm eff} = 3280 \pm 87$ K. The uncertainties are evaluated by a Monte Carlo simulation. For the calibration stars in Table 3, the standard deviation in $T_{\rm eff}$ is ±31 K and agrees with the assumed error estimates of Levesque et al. (2005). The agreement between our indirect derivation of $T_{\rm eff}$ and direct interferometric measures (Table 1) is convincing.

Therefore, we utilize this calibration for determining $T_{\rm eff}$, and calculate the temperature for individual values of γ_2 at any given epoch for α^1 Her. The observed maximum and minimum values of γ_2 are 1.500 and 1.881 mag, respectively. Consequently, the upper and lower limits of the effective temperature of α^1 Her are $T_{\rm eff} = 3365$ K and 3155 K, respectively; they correspond to inferred spectral types of ∼M5 and M6, respectively. This temperature variation indicated by the variability in the γ_2 index can be induced by pulsations. This can be seen from the inferred variations of the star's radius and luminosity (Figure 2). However, smaller non-periodic contributions to this variability could arise from the growth and decline of starspots from the changes in $T_{\rm eff}$ produced by the presence of large convective cells in the star's atmosphere (Stothers 2010).

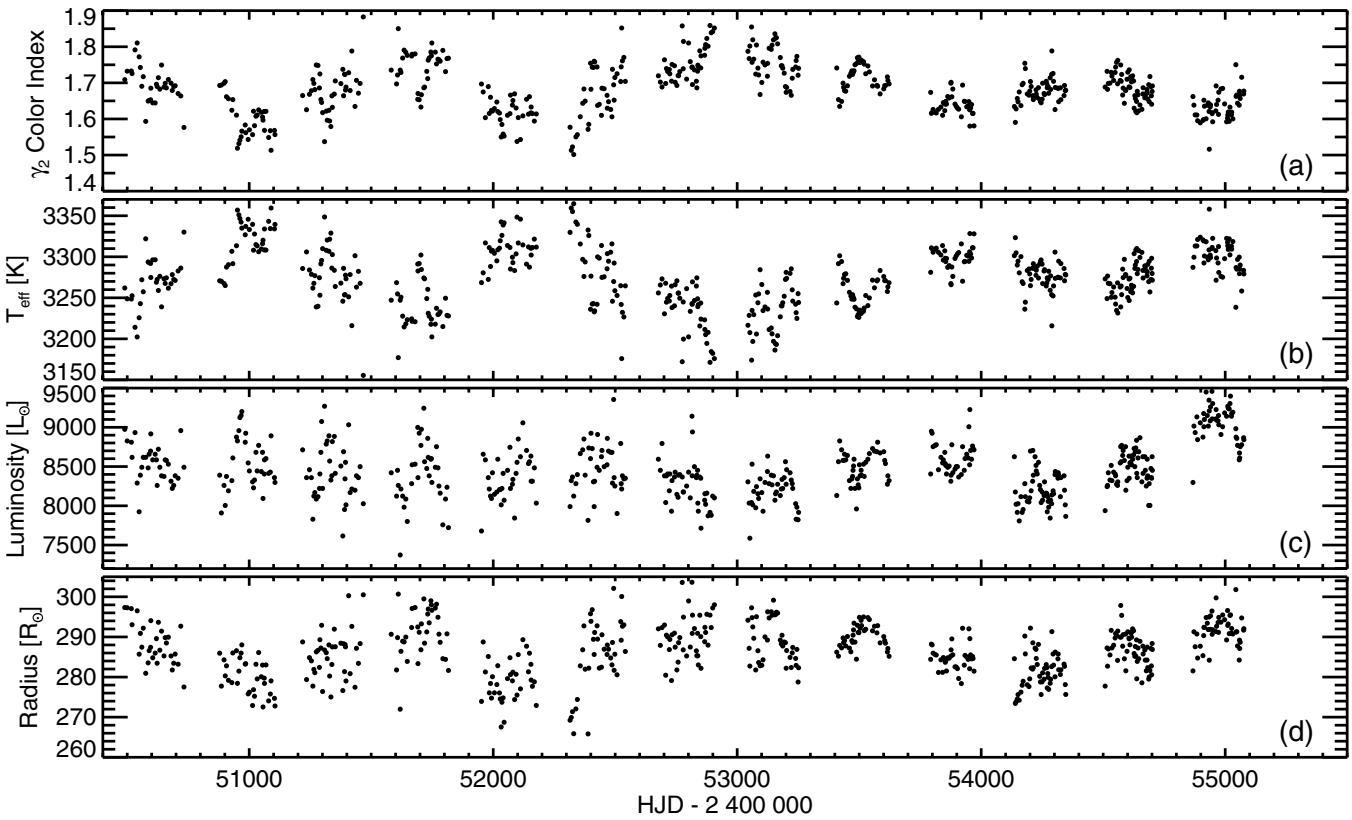

Figure 2. Temporal variation in the γ_2 color index (a), effective temperature (b), luminosity (c), and radius (d). The variability with the period of LSP (∼1400 days) in all physical parameters is evident. See also Equations (5), (7), (8), and (9). The full light curves are published in Appendix A (Figure 11).

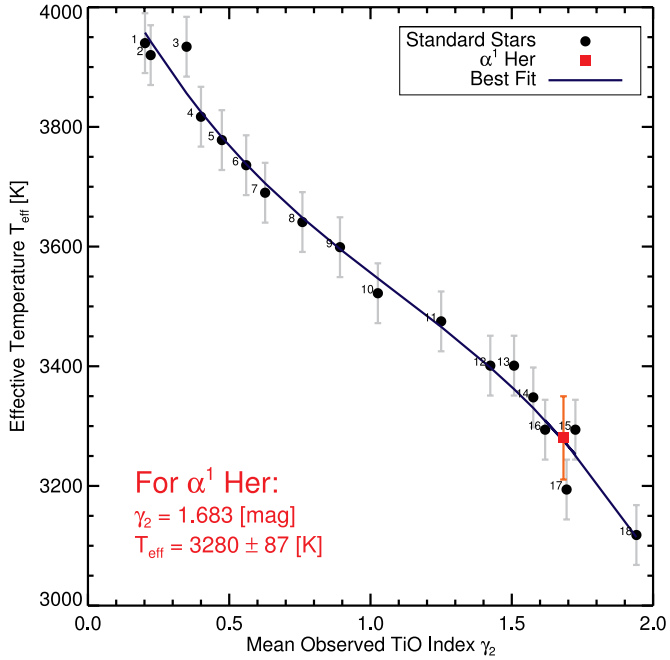

Figure 3. $T_{\rm eff}$ calibration with 18 mid-K to late-M standard stars selected from Wing (1978). Filled circles designate the stars from Table 3 marked with their associated ID. The solid curve is the polynomial fit from Equation (6). The red square represents α^1 Her.

(A color version of this figure is available in the online journal.)

6. TIME VARIABILITY OF LUMINOSITY AND RADIUS

Once the change in the color temperature is accounted for, the calculation of luminosity and radius is straightforward from the Stefan–Boltzmann law $L/L_\odot = (R/R_\odot)^2\,(T/T_\odot)^4$. Lattanzio & Wood (2004) and Unno et al. (1989) argue that this relation yields reliable results for the AGBs. With a different calibration, the same law is employed in interferometric observations of nearby Miras and supergiants as a means of direct measurement of their luminosity and radius (e.g., Weiner et al. 2003; Perrin et al. 2004; Lacour et al. 2009). Therefore,

$$m_{\rm bol} = C + {\rm BC_C} \tag{7}$$

$$M_{\rm bol} = m_{\rm bol} - 5.207 \tag{8}$$

$$L/L_\odot = 10^{(4.75-M_{\rm bol})/2.5}, \tag{9}$$

where $M_{V\odot} = 4.75$ is the absolute magnitude of the Sun (Allen 1976), 5.207 is the distance modulus to the α Her system from *Hipparcos* (Equation (1)), and ${\rm BC_C} = 1.735 \pm 0.030$ mag is the bolometric correction to the Wing C filter (Appendix B). The ISM absorption in the Wing C filter along the α Herculis line of sight was deemed insignificant. Dyck et al. (1996) also assume zero extinction in near-IR toward the α Herculis system.[6] From Table 2 and Appendix B, the bolometric apparent magnitude has a net error of $\Delta m_{\rm bol} \approx 0.036 + 0.002 = 0.038$; therefore, a rough estimate of the uncertainty in the absolute bolometric magnitude is $\Delta M_{\rm bol} = \Delta m_{\rm bol} + (5/\ln 10)(\Delta d_{\rm Hip}/d_{\rm Hip}) = 0.35$ mag, and that of luminosity is $\Delta \log(L/L_\odot) = \Delta M_{\rm bol}/2.5 = 0.14$ dex. The radius variation from the Stefan–Boltzmann law is

$$R/R_\odot = (L/L_\odot)^{1/2}(T_{\rm eff}/5779)^{-2} \tag{10}$$

[6] However, we are aware that this can impose a bias in the inferred bolometric luminosity.

Table 4
Extrema Measures of $T_{\rm eff}$ (°K), $L/L_\odot$, and $R/R_\odot$ for α^1 Her

	Mean	Min	Max	δ
$T_{\rm eff}$ (°K)	3280 ± 87	3155	3365	6.4%
$\log(L/L_\odot)$	3.92 ± 0.14	3.86	3.97	25.8%
$R/R_\odot$	284 ± 60	264	303	13.9%

Note. See Equations (6)–(10).

and the relative error in the radius is approximately 21%.

Figures 2(a)–(d) show how the time dependence of the TiO index γ_2 is translated to temporal variations in physical quantities of the star $T_{\rm eff}$, $L/L_\odot$, and $R/R_\odot$ with the period of the LSP. When the star is hotter, it is more luminous and smaller. Apparently, stellar pulsation is the most likely mechanism to explain the observed simultaneous variability in the temperature, luminosity, and radius of the star (Wood et al. 2004; Nicholls et al. 2009). This will be a subject of a forthcoming paper.

Table 4 summarizes the minimum, maximum, and average values for these calculated quantities; in the last column, $\delta = |{\rm Max}-{\rm Min}|/{\rm Mean}$ is the relative change in any quantity during our observations. Our derived luminosity is close to the lower limit of Perrin et al. (2004; see Table 1) and agrees within the error bars. The angular diameter of the star based on Equations (1), (2), and (10) is 23.95 ± 5.03 mas; this is 24% less than the K-band angular diameter measure of Perrin et al. (2004; see Table 1). Despite the significant disagreement between our inferred angular diameter of α^1 Her and that of the literature (Table 1), we show in Section 8.3 that our radius assessment has a better agreement with our evolutionary models.

7. MODELING THE α HERCULIS STARS

Based on the measurements collected from the literature and within their corresponding uncertainties (Table 1), we model the three stars using the state-of-the-art stellar structure and evolution code MESA[7] (v.4589; Paxton et al. 2011, 2013). We assume that the three stars of the α Herculis system are coeval. We adopt the Solar chemical composition of Asplund et al. (2009), i.e., $(X, Y, Z) = (0.720, 0.266, 0.014)$ (see Table 1 in Ekström et al. 2012 and details therein). This choice is supported by the spectroscopy of Hoflich et al. (1986). The differences among spectroscopic classes of α Herculis stars (Table 1) imply that their initial ZAMS masses are different.

7.1. Rotational Mixing

The initial equatorial rotation rates of α Herculis stars are unknown a priori. Therefore, we set up a dense grid (in initial mass) of evolutionary models that take into account the shellular rotation (Heger et al. 2000, 2005). Yet, the choices for the initial rotation rates could be various (compare, e.g., Tassoul 2000; Charbonnel & Lagarde 2010; Cantiello & Langer 2010). Similar to Lagarde et al. (2012), we adopt $\eta_{\rm rot} = \Omega_{\rm eq}/\Omega_{\rm cri} = 0.45$ on the ZAMS, where the critical angular velocity is $\Omega_{\rm cri} = (8GM/27R_{\rm eq}^3)^{1/2}$. $R_{\rm eq}$ is the equatorial radius calculated for a non-rotating case, and M is the stellar mass.

[7] Modules For Experiment in Stellar Astrophysics (MESA) is an open-source code accessible from http://mesa.sourceforge.net. The Fortran 90 inlists and modules that we used are also available via http://mesastar.org/.

7.2. Convection, Overshooting, and Thermohaline Mixing

The mixing processes near the stellar core have an appreciable effect on the duration and width of the main-sequence (MS) phase in the HR diagram (Maeder 2009). For our case, the mixing parameters of α^2 Her B critically influenced the age of this star. The convective mixing is treated using the Mixing Length Theory (MLT) of Böhm-Vitense (1958), with $\alpha_{\rm MLT} = 1.6$. Boundaries of the convective zone(s) are located where $\nabla_{\rm rad} = \nabla_{\rm ad}$. The overshooting beyond the boundaries of convective zones is included with the extent of the overshoot zone a multiple of the local pressure scale height, $d_{\rm ov} = \alpha_{\rm ov} H_p$ with $\alpha_{\rm ov} = 0.10$.

Thermohaline mixing has been recently discussed as a source of extra mixing in models of red giant branch (RGB) stars. MESA uses the formulation by Kippenhahn et al. (1980) and Traxler et al. (2011). For applications, see Cantiello & Langer (2010) and Charbonnel & Lagarde (2010). Two-dimensional and three-dimensional hydrodynamic simulations of this double-diffusive instability indicate a very slow mixing process acting in low-mass stars (Denissenkov 2010; Denissenkov & Merryfield 2011; Traxler et al. 2011). Thus, while this might have an impact on observable surface abundances, the effect on the internal thermal structure (hence luminosity and stellar age) is predicted to be negligible (Denissenkov & Pinsonneault 2008). In this study, we ignore the thermohaline mixing. Furthermore, we also ignore the extra mixing induced by magnetic fields, but we do include the radiative levitation based on Thoul et al. (1994) and Morel & Thévenin (2002).

7.3. Mass Loss

Dust-driven mass loss from highly luminous cool stars depends sensitively on the mass, radius, luminosity, and metallicity of the star (e.g., van Loon 2006). We employ the Reimers (1977) criteria for RGB mass loss, and the prescription by Blöcker (1995) on the AGB phase:

$$\begin{aligned} \dot{m} &= 1.4 \times 10^{-13}\, \eta_{\rm RGB}\, (L/gR); & \eta_{\rm RGB} &= 0.5, \\ \dot{m} &= 4.83 \times 10^{-9}\, \eta_{\rm AGB}\, (L^{2.7}/M^{2.1}); & \eta_{\rm AGB} &= 0.1, \end{aligned} \tag{11}$$

with L and M expressed in solar units. The transition between the two prescriptions is made when the He mass fraction in the core is less than 10^{-3}. The rotationally enhanced mass-loss rate is employed, similar to Maeder & Meynet (2001).

8. RESULTS

8.1. The Composite HR Diagram of the α Herculis System

We calculate a dense grid of evolutionary models composed of 55 tracks. The employed mass range M and stepsize in units of Δ_M in $M_\odot$ is

$$\begin{aligned} M &: 1.300 \cdots 1.500, & \Delta_M &= 0.100 \\ M &: 1.600 \cdots 2.300, & \Delta_M &= 0.025 \\ M &: 2.500 \cdots 8.000, & \Delta_M &= 0.250. \end{aligned} \tag{12}$$

For every track, the evolution calculation is stopped after the core helium depletion (hereafter CHeD), when $T_{\rm eff}$ drops below 3100 K. At the end, the grid consists of more than 353,000 rows and 162 columns of evolutionary information, such as $T_{\rm eff}$ and L. The synthetic absolute bolometric magnitude $M_{\rm bol}$, V-band bolometric correction B.C., and the standard Johnson–Cousins $UBV\,RI\,JHKLL'M$ color indices are calculated based on Lejeune et al. (1998). The grid in its entirety is

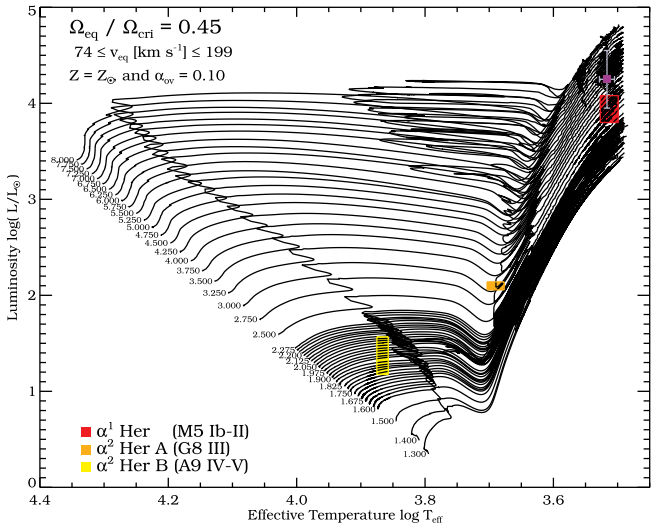

Figure 4. MESA grid of rotating low- to intermediate-mass stars from the MS phase up to the AGB phase (CHeD and $T_{\rm eff} \leqslant 3100$ K) at solar metallicity. The initial rotation rate is $\eta_{\rm rot} = 0.45$. The positions of the three members of the system are highlighted based on Tables 1 and 4.

(A color version of this figure is available in the online journal.)

bundled as a single tar file, and can be retrieved in the online journal. For a detailed description of the data columns per each track, refer to the included ReadMe file. The grid is sketched in Figure 4. The positions of the three α Herculis members within their 1σ boxes of uncertainty are highlighted based on entries in Table 4; the result of Perrin et al. (2004) is also overplotted.

8.2. Constraining the Age of the α Herculis System

From Figure 4 and the measured physical properties of α^2 Her B (in Table 1 and Section 3), this A9 IV-V star is either in the core hydrogen-burning phase or has just entered the sub-giant phase. Hence, it is the least evolved (and least massive) member of the system. Because the main-sequence evolution of stars is understood with more certainty (see Langer 2012), the model inference for α^2 Her B is more robust than for the other two components. Consequently, we base the estimate of the *age* of the system on the age we infer for the A9 IV-V star α^2 Her B. In other words, we assume that the only reason for the differences in evolutionary status of the three α Herculis stars lies in their differences in initial mass.

Figure 5 enlarges a small portion of the grid (i.e., Figure 4), and shows models with their respective luminosity and effective

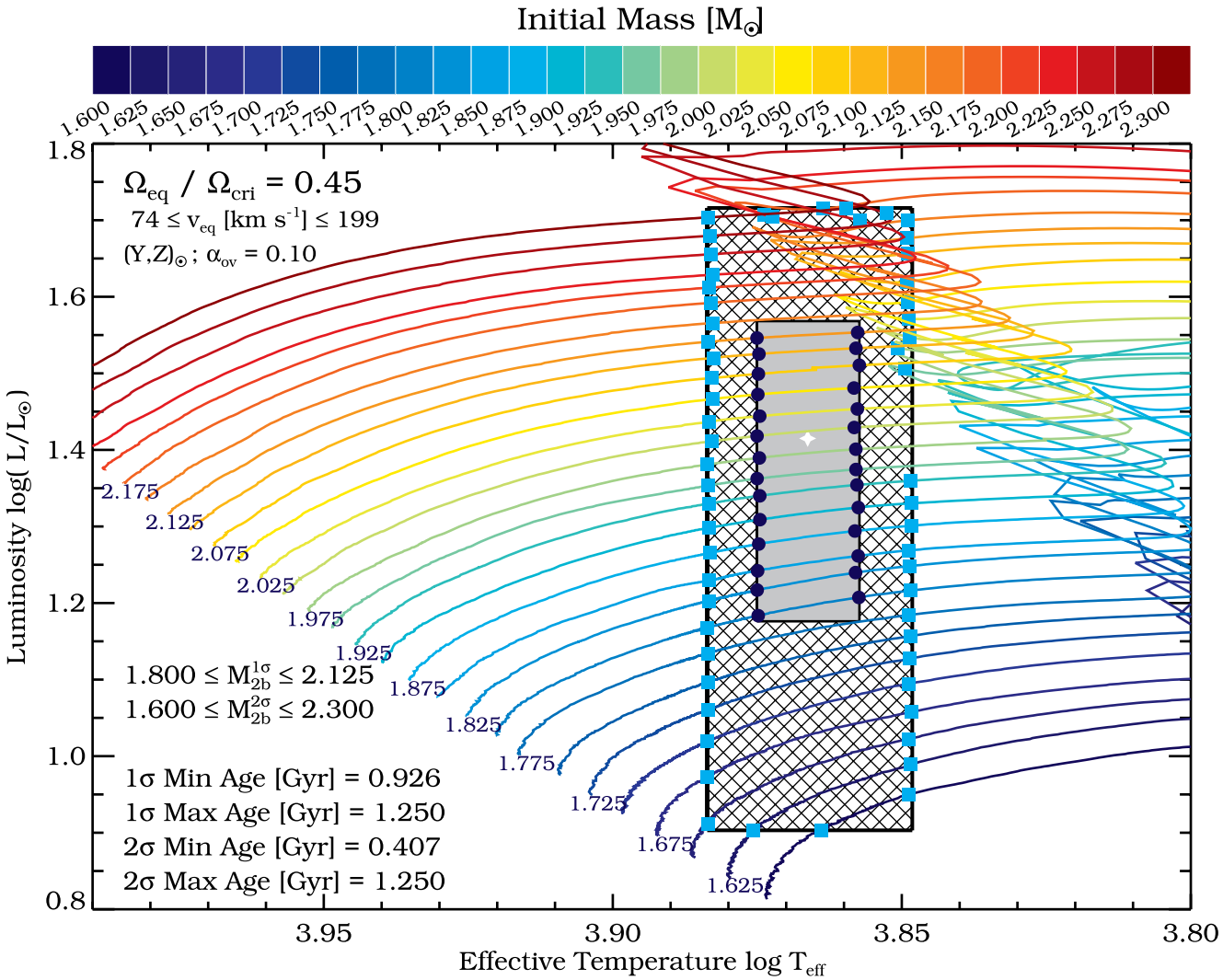

Figure 5. Close zoom into Figure 4 shows MESA tracks of α^2 Her B within its observed 1σ and 2σ range of $T_{\rm eff}$ and $\log(L/L_\odot)$ (Table 1). The age and mass of this star inferred from its position on HR diagram are listed in Table 5 and Equation (14), respectively. The color coding is based on the initial mass for each track.

(A color version of this figure is available in the online journal.)

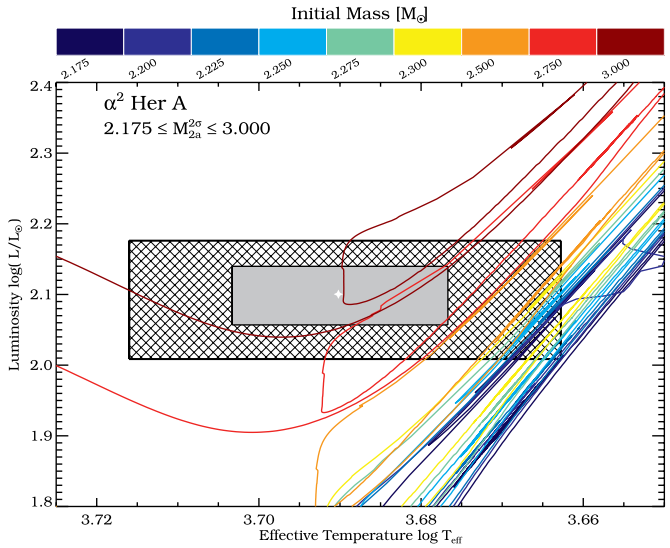

Figure 6. MESA tracks of α^2 Her A, within the 2σ observed range of $T_{\rm eff}$, luminosity, and ages from Table 5. Equation (15) gives the possible mass of this star. The color coding is based on the initial mass for each track.

(A color version of this figure is available in the online journal.)

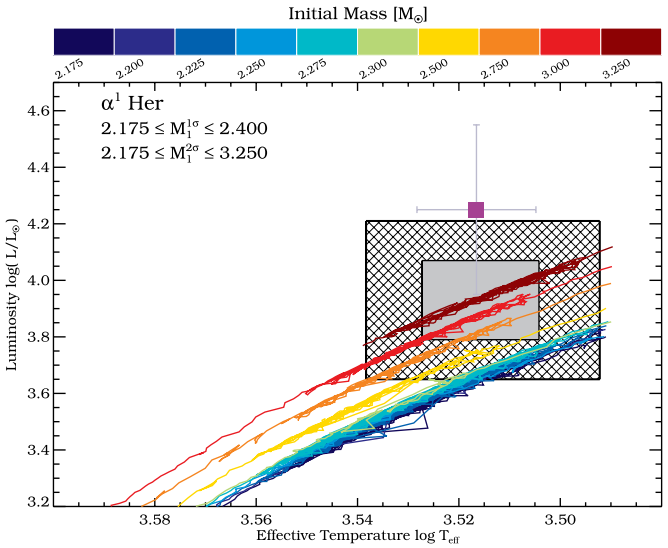

Figure 7. MESA tracks of α^1 Her within the observed range of temperatures and luminosities (Table 1), and ages constrained from α^2 Her B (Figure 5 and Table 5). The observation with error bars is reproduced from Perrin et al. (2004). The color coding is based on the initial mass for each track.

(A color version of this figure is available in the online journal.)

Table 5
Model Age Estimation for α^2 Her B

Uncertainty	Minimum (Gyr)	Maximum (Gyr)
1σ	0.926	1.250
2σ	0.407	1.250

temperature lying in the 1σ (filled gray) and 2σ (cross hatched) boxes of uncertainty for α^2 Her B (see Table 1). The filled symbols mark where the tracks enter/exit the highlighted zones, and where we measure the model ages. The lower and upper age limits of the system are assessed based on the age at these flagged points. We address these as the *age constraints*. Our results within the 1σ and 2σ uncertainties in $T_{\rm eff}$ and $\log(L/L_\odot)$ are summarized in Table 5. The timesteps (around the flagged points in Figure 5) are approximately two orders of magnitude smaller than the inferred ages.

We repeat the same procedure for the M12 tracks. For the age of α^2 Her B, we find different results: with 1σ uncertainty, the age ranges from 0.787 to 1.452 Gyr, and similarly, with 2σ uncertainty it ranges from 0.734 to 1.719 Gyr. With respect to M12, the MESA ages roughly differ by 14% to 53%. We cannot extend this comparison to E12 and L12 tracks, as their coarse mass spacing does not allow it. In Section 8.4, we address this age comparison again.

8.3. Masses of α Herculis Stars from the HR Diagram

We designate the initial masses of α^1 Her, α^2 Her A, and α^2 Her B as M_1, $M_{2\rm a}$, and $M_{2\rm b}$, respectively. From the assumption that the differences in the current evolutionary status of α Herculis stars have their origins in their initial masses, M_1, $M_{2\rm a}$, and $M_{2\rm b}$ must obey the inequality

$$M_{2\rm b} < M_{2\rm a} < M_1. \tag{13}$$

From Figure 5, it is straightforward to find the most viable mass for α^2 Her B

$$\begin{aligned} 1.800 \leqslant M_{2\rm b}^{1\sigma}\ [M_\odot] \leqslant 2.125, \\ 1.600 \leqslant M_{2\rm b}^{2\sigma}\ [M_\odot] \leqslant 2.300. \end{aligned} \tag{14}$$

M12 tracks, strikingly, give $1.80 \leqslant M_{2\rm b}^{1\sigma}\ [M_\odot] \leqslant 2.10$ and $1.60 \leqslant M_{2\rm b}^{2\sigma}\ [M_\odot] \leqslant 2.30$, in close agreement with Equation (14). Due to the coarse mass spacing in E12 and L12, we decide not to assess masses from their tracks.

We permitted models with slightly higher masses than in Equation (14) to deplete their core helium content, to ascend the AGB, and to reach $T_{\rm eff} \leqslant 3100$ K. Our strategy is to tightly bind M_1 and $M_{2\rm a}$ within 1σ (and 2σ) uncertainties to find those tracks that *simultaneously* match the observed $T_{\rm eff}$ and $\log L$ of these stars, in addition to their ages lying between the minimum and maximum age of the system from Table 5. Figure 6 shows α^2 Her A on the HRD. Only the tracks within the 2σ box can satisfy the above conditions; therefore, the initial mass range for this star is

$$2.175 \leqslant M_{2\rm a}^{2\sigma}\ [M_\odot] \leqslant 3.000, \tag{15}$$

where the uncertainty is not larger than $0.05\,M_\odot$. One of the following evolutionary scenarios applies to α^2 Her A: it is ascending the RGB, has just ignited helium in the core, or is on the early-AGB phase.

Figure 7 shows the expected location of the primary α^1 Her on the HRD based on the observations of Perrin et al. (2004) and the present work (Tables 1 and 4). There is reasonable agreement of the luminosity of the primary star with the two approaches. Similar to the previous stars, we assess the evolutionary initial mass of the primary based on its age and location on the HRD as

$$\begin{aligned} 2.175 \leqslant M_1^{1\sigma}\ [M_\odot] \leqslant 2.400, \\ 2.175 \leqslant M_1^{2\sigma}\ [M_\odot] \leqslant 3.250. \end{aligned} \tag{16}$$

The solar-type pulsation pattern in the primary is already established (Bedding 2003; Kiss et al. 2006; Moravveji et al. 2010). Based on this fact, we earlier estimated the mass of this star to be $2.5^{+1.6}_{-1.1}\ M_\odot$ (Moravveji et al. 2011) using the asteroseismic mass and radius scaling laws (Huber et al. 2011). Though the sizes of the uncertainties are large, the seismic mass is consistent with Equation (16). In Sections 8.4 and 8.5,

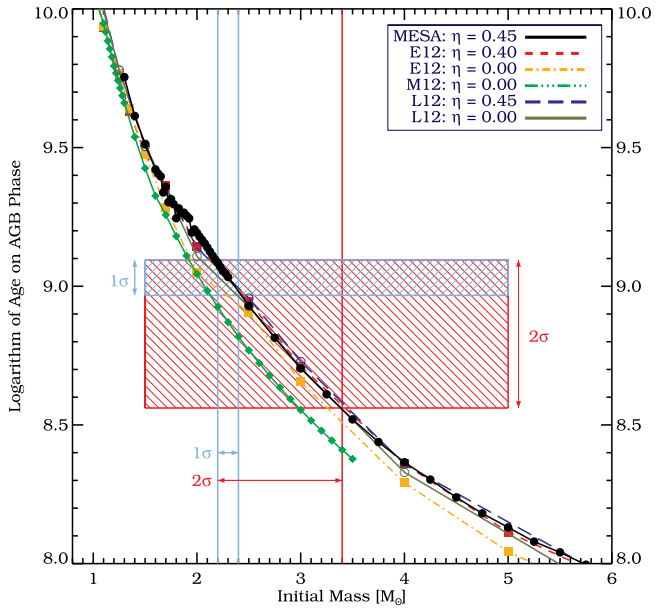

Figure 8. Comparison of stellar age vs. initial mass between MESA, E12, L12, and M12. The plotting symbols distinguish between different codes and their corresponding $\eta_{\rm rot}$. The highlighted box marks the expected age of the α Her system from Table 5.

(A color version of this figure is available in the online journal.)

we attempt to examine Equation (16) based on the surface abundances of the primary.

It is worthwhile to mention that the model radius for α^1 Her based on our grid lies in the range $200 \lesssim R/R_\odot \lesssim 314$. This agrees better with our inferred radius in Table 4 than with the near-IR interferometric estimate (Equation (3)). We admit that our treatments of the envelope convection and that of the extended atmosphere of AGB stars in our MESA models are simplistic.

8.4. Agreement in AGB Age Assessment

Figure 8 shows the final (i.e., AGB) lifetime of tracks from MESA, E12, L12, and M12 versus their corresponding initial masses. The ages given by M12 (green line) are significantly less than the rest of models, as the tracks terminate on the sub-giant phase. On the higher-mass regime, the lifetime of rotating star tracks in logarithmic scale is about 0.1 dex higher than the non-rotating star tracks. This is explained by extra engulfment of hydrogen fuel by the rotating core during the MS phase. Among evolution tracks including rotation, those of L12 have higher ages.

The highlighted 1σ and 2σ boxes in Figure 8 show the upper and lower bounds of the age of the α Herculis system from Table 5. The vertical lines show the initial masses of stars that can reach the AGB phase within the given age (in agreement with Equation (16)). Based on this, the age constraint from Table 5 is robustly independent of the stellar evolution code used. This places α^1 Her among the few AGB stars in our galaxy with known ages.

8.5. Surface Abundance Ratios of Carbon and Oxygen Isotopes

The literature on the spectroscopic abundance analyses of α^1 Her is surprisingly scarce. Harris & Lambert (1984) measure the surface ratios of the key CNO processed species in the atmosphere of α^1 Her. They are $^{12}{\rm C}/^{13}{\rm C} = 17 \pm 4$, $^{16}{\rm O}/^{17}{\rm O} = 180^{+70}_{-50}$, and $^{16}{\rm O}/^{18}{\rm O} = 550^{+225}_{-175}$. The large uncertainty in the latter is not constraining, and we exclude it from our analysis. To our knowledge, there is no record of the detection of Li and/or Tc on α^1 Her; we conservatively interpret this as due to the hot bottom burning not occurring in α^1 Her and the mass being below nearly $\sim 4\,M_\odot$. This complies with Equation (16).

El Eid (1994) employed these abundance ratios, and concluded that the mass of α^1 Her is within 5–7 $M_\odot$. However, the models calculated by El Eid did not include rotational and overshooting mixing. During the past two decades, there have been major improvements in the input physics to the stellar evolution codes, mainly to the opacity, EOS, and nuclear reaction rates. For this reason, we repeat the same exercise as in El Eid (1994) with MESA.

Figure 9 shows the surface abundance ratios of $^{12}{\rm C}/^{13}{\rm C}$ (left panel) and $^{16}{\rm O}/^{17}{\rm O}$ (right panel) versus the initial model masses. We designate these by r_1 and r_2, respectively. The observations from Harris & Lambert (1984) within the 1σ and 2σ uncertainties are highlighted. These two ratios magnify the net contribution from convective and extra mixing mechanisms during the evolution history of the models. We compare the same yields from MESA, E12, and L12 for their rotating and non-rotating tracks. For the large departure of $v_{\rm eq}$ in L12 from MESA and E12, we subsequently present but do not discuss the surface abundance ratios from their rotating stellar tracks.

An inspection of the $r_1 = {}^{12}{\rm C}/^{13}{\rm C}$ ratio (Figure 9, left) indicates the different predictions made by different codes. In E12, r_1 declines monotonically with the model mass (orange and red squares). The inclusion of rotation gradually mixes extra ^{13}C to the surface, and r_1 is smaller for rotating tracks compared to their non-rotating counterparts. The non-rotating case of L12 (green empty circles) follows the same trend as E12. In MESA (black filled circles), r_1 is irregular on the low-mass regime and then exhibits a clear variable trend on the higher-mass end. Thus, it is not straightforward to assess the 1σ and/or 2σ mass of α^1 Her with any certainty.

The $r_2 = {}^{16}{\rm O}/^{17}{\rm O}$ ratio (Figure 9, right) shows nearly the same behavior in all codes except MESA: declining sharply with increasing model mass, reaching a dip around $\sim 2\,M_\odot$, and rising again. In E12, the gradual surface enrichment of ^{17}O by rotation during the MS enforces a deeper dip. The results of L12 are roughly between those of E12. In MESA, the combined effects of atomic diffusion and rotational mixing result in the highest surface ^{17}O enrichment, which suppresses r_2. For massive AGBs, the MESA predictions differ from the other models. Once more, the mass assessment for α^1 Her is not necessarily in agreement between different codes: with the rotating E12 tracks, we find $1.4 \lesssim M_1^{2\sigma} \lesssim 4.2$, with L12 we find $1.4 \lesssim M_1^{2\sigma} \lesssim 3.2$, and with MESA we find $2.9 \lesssim M_1^{2\sigma} \lesssim 5.3$. We find none of the mass assessments in good agreement with the predictions of Equation (16). Therefore, we do not succeed in fine-tuning M_1 by using surface abundance ratios r_1 and r_2.

9. DISCUSSION AND CONCLUDING REMARKS

In Sections 5 and 6, we propose a photometric method using Wing ABC filters to exploit the effective temperature (Equation (6)) and luminosity (Equations (7)–(9)) of evolved—mid-K to mid-M spectral type—stars in agreement with near-IR interferometry. On one hand, direct measurement of angular diameter and $T_{\rm eff}$ for stars based on long-baseline interferometry has some shortcomings.

1. There are currently few actively operating interferometers that are accessible for the broad astronomy community.

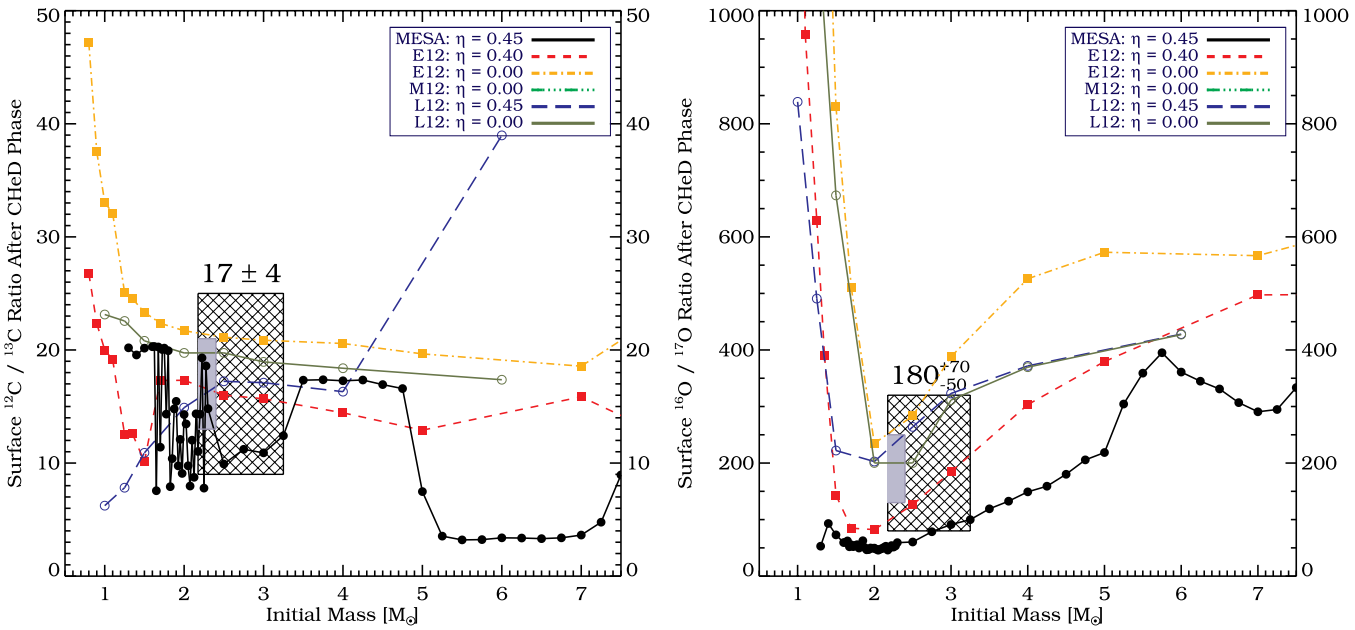

Figure 9. Variation of the surface abundance ratios of $^{12}C/^{13}C$ (left) and $^{16}O/^{17}O$ (right) with initial ZAMS masses for an M5 AGB star. We compare similar predictions from MESA, Ekström et al. (2012, E12), and Lagarde et al. (2012, L12), and for different choices of initial rotation rate η_{rot}. For α^1 Her, the measured ratios within 1σ and 2σ boxes from Harris & Lambert (1984) are highlighted with shaded and hatched strips, respectively. The mass intervals are adopted from Equation (16).

(A color version of this figure is available in the online journal.)

2. A limited number of stars fall within the observability of current instruments, according to their apparent magnitude and apparent angular diameter.

On the other hand, our proposed small-aperture photometry does not suffer these limitations, and can be applied to individual evolved stars.

To deduce the mass and age of α Herculis stars, we used a grid of stellar evolutionary tracks. The assumptions, simplifications, and uncertainties in the physical parameters of the model translates into significant uncertainties in calculating model masses, radii, and ages. Basu et al. (2012) provide an in-depth analysis of these grid-based approaches. They estimate that the accuracy of mass evaluation without inclusion of additional seismic information is at least 8%. We conclude from Figure 8 that the model ages and masses calculated by MESA, E12, L12, and M12 are in satisfactory agreement. This is not a surprise as far as the four codes we are comparing employ very similar nuclear reaction rates.[8] This result supports the stringency of model-dependent age determination approaches, such as asteroseismology of red giants in clusters (Basu et al. 2011; Miglio et al. 2013).

Figure 10 summarizes our results on the mass distribution in the α Herculis system within 1σ and 2σ uncertainties. It is a collection of the results from Equations (14)–(16), which employ the position of α Herculis stars on the HRD (from Figures 5–7) and the age constraint (Table 5). From the condition that the masses of α Herculis stars must not overlap (Equation (13)), we have no additional information that would limit the mass ranges for components of the α Herculis system.

Figure 9 shows very different patterns for $^{12}C/^{13}C$ and $^{16}O/^{17}O$ atmospheric abundance ratios. It is difficult to judge whether the observed differences between the $^{12}C/^{13}C$ and

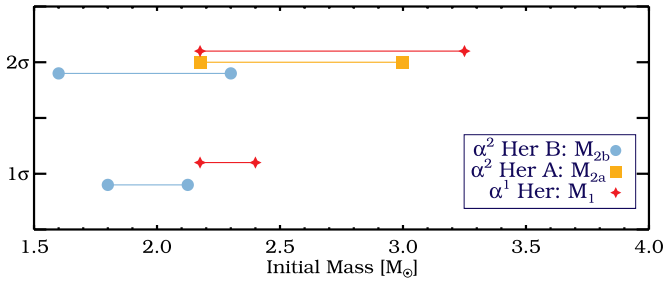

Figure 10. Distribution of stellar mass in the α Herculis system. See the text and Equations (14)–(16) for explanations. Yet, we cannot apply Equation (13) to set more strict limits on the mass of each star in the system. The mass assessment from Figure 9 is non-constraining.

(A color version of this figure is available in the online journal.)

$^{16}O/^{17}O$ trends in different codes are more of a physical nature or of computational origin; this is beyond the scope of this study. Yet, it calls for an observational calibration of surface abundances versus the global stellar parameters, such as mass and $\log g$, which in return requires a high-precision mass assessment. The asteroseismology of oscillating red giants comes to the rescue, as it can indirectly provide measures of $\log g$ from seismic scaling laws as precise as $\sim$1% (see, e.g., Basu et al. 2011; Morel et al. 2013; Thygesen et al. 2012). Once this is relaxed, surface abundance ratios might serve as an alternative technique in estimating the masses of stars when seismic and/or binarity information is missing.

10. SUMMARY

We carried out more than two decades of multicolor photometry of the nearby triple-stellar system, α Herculis, and devise a method to extract the effective temperature and bolometric luminosity of the primary star. For this, we use Wing ABC filters. For α^1 Her, we determine average values of $T_{\rm eff} = 3280 \pm 87$ and

[8] All employed codes in this study use NACRE (Angulo et al. 1999) thermonuclear reaction rates with updates to $^{14}N(p,\gamma)^{16}O$, triple-α, $^{14}N(\alpha,\gamma)^{18}F$, and $^{12}C(\alpha,\gamma)^{16}O$ reactions.

Table 6
Wing (1978) Calibration Stars Used to Compute Wing C-filter Magnitude Corrections

HR Number	Spectral Type	V (mag)		BC_V (mag)		Wing 1040 nm (mag)		BC_C (mag)
(a)	(b)	(a)		(Equation (A3))		(b)		(Equation (A1))
85	M4.8	5.12	+	(−2.345)	−	0.97	=	1.805
1722	M4.8	5.65	+	(−2.345)	−	1.71	=	1.595
4949	M4.8	5.66	+	(−2.345)	−	1.53	=	1.785
7804	M4.8	5.55	+	(−2.345)	−	1.60	=	1.605
4045	M4.9	6.30	+	(−2.382)	−	2.15	=	1.768
5192	M5.0	4.19	+	(−2.419)	−	(-0.03)	=	1.801
587	M5.1	5.51	+	(−2.457)	−	1.31	=	1.743
4909	M5.1	5.84	+	(−2.457)	−	1.60	=	1.783
Ave. Spec.	M4.9					Average	=	1.735
						Std. Dev.	=	0.085
						Std. Err.	=	0.030

References. (a) Hoffleit & Jaschek 1982; (b) Wing 1978.

$\log(L/L_\odot) = 3.92 \pm 0.14$. These agree with the near-infrared interferometric observations of Perrin et al. (2004) within the error bars.

We calculated a grid of 55 evolutionary tracks with MESA that incorporate the effects of stellar rotation. The grid has a solar composition, and is calculated for the mass range 1.30 $M_\odot$ to 8.0 $M_\odot$. Within 2σ uncertainty, the α Herculis system has an age of 0.41 to 1.25 Gyr. The inferred model age from MESA agrees with the E12 and L12 tracks. We consequently find that the initial masses of the stars in the α Herculis system are distributed between 1.60 and 3.40 $M_\odot$, with the primary M5 Ib-II AGB star having a mass $2.175 \leqslant M_1 \leqslant 3.250$. This result was independently reproduced by Moravveji et al. (2011) by extending the seismic scaling relations for RGBs to AGB stars. This now settles the debates on the mass of α^1 Her indicating a smaller value than formerly thought, and rejects its evolutionary status as a more massive red supergiant (like α Ori and α Sco; see Section 2).

Soon, *Gaia* will provide precise parallaxes for nearly half a million Galactic stars. Multicolor photometry of M-type giants and supergiants in Wing ABC filters, when combined with such precise parallaxes, can provide the stellar effective temperatures and luminosities at a precision comparable to or even better than the infrared interferometry. Also, in the future it should be possible to measure the total mass of the α Herculis system by determining its orbital elements. Interferometric measures, when combined with past astrometric measures (see Baize & Petit 1989), could eventually yield a definite orbital period and semimajor axis that result in a direct measure of the system's total mass.

We appreciate the comments from the anonymous referee that helped us improve this manuscript. We thank Andrej Prša for granting us access to the Villanova University computing facility, and Thomas Lebzelter, Achim Weiss, and Graham Harper for reading and commenting on this document. E.M. is grateful to Bill Paxton and Falk Herwig for many fruitful discussions about MESA, and also to the board of MESA for freely publishing the code. We acknowledge using the Coyote IDL graphics packages made freely available by David Fanning. The research leading to these results has received funding partly from the European Research Council under the European Community's Seventh Framework Programme (FP7/2007–2013)/ERC grant agreement No. 227224 (PROSPERITY), and partly by the NSF/RUI grant AST-1009903 to Villanova University that we gratefully acknowledge.

APPENDIX A

LIGHT CURVES IN JOHNSON *VRI* AND WING ABC FILTERS

The small-aperture photometric data for the α Herculis system is collected from two sites, and it spans over 23 years. Figure 11 represents the multi-site, multi-color photometry of the α Herculis system. For more details, refer to Section 4 and Table 2.

APPENDIX B

WING C-FILTER BOLOMETRIC CORRECTION BC_C

The C filter of Wing's three-color system is centered in a continuum region free from strong absorption lines (see Figure 1 and Table 2). The central wavelength is at 1040 nm with an FWHM of 42 nm (White & Wing 1978). The transmitted flux through the filter measures near-IR apparent magnitudes that approximate bolometric magnitudes, as seen in Mira-variable light curves near their energy maxima (Wing 1992). Bolometric corrections BC_C between 1040 nm magnitudes and the *UBV*-based apparent bolometric magnitudes are computed for eight M4.8 to M5.1 calibration stars via Equation (A1),

$$BC_C = m_{bol} - m_{1040}, \quad \text{(A1)}$$

where m_{1040} is the 1040 nm magnitude and is taken from Wing (1978) for each star. The *UBV*-based apparent bolometric magnitude, m_{bol}, is calculated from Equation (A2):

$$m_{bol} = V + BC_V. \quad \text{(A2)}$$

The *V*-band magnitudes are taken from the Bright Star Catalog (Hoffleit & Jaschek 1982) or the Simbad Astronomical Database. Using the bolometric corrections in Table 5 of Levesque et al. (2005), a second-order polynomial is generated to calculate unique bolometric corrections that are dependent on the spectral sub-types of the eight calibration stars. This second-order polynomial is given in Equation (A3),

$$BC_V = -0.0282x^2 - 0.039x - 1.1703, \quad \chi^2_{red} = 0.9821, \quad \text{(A3)}$$

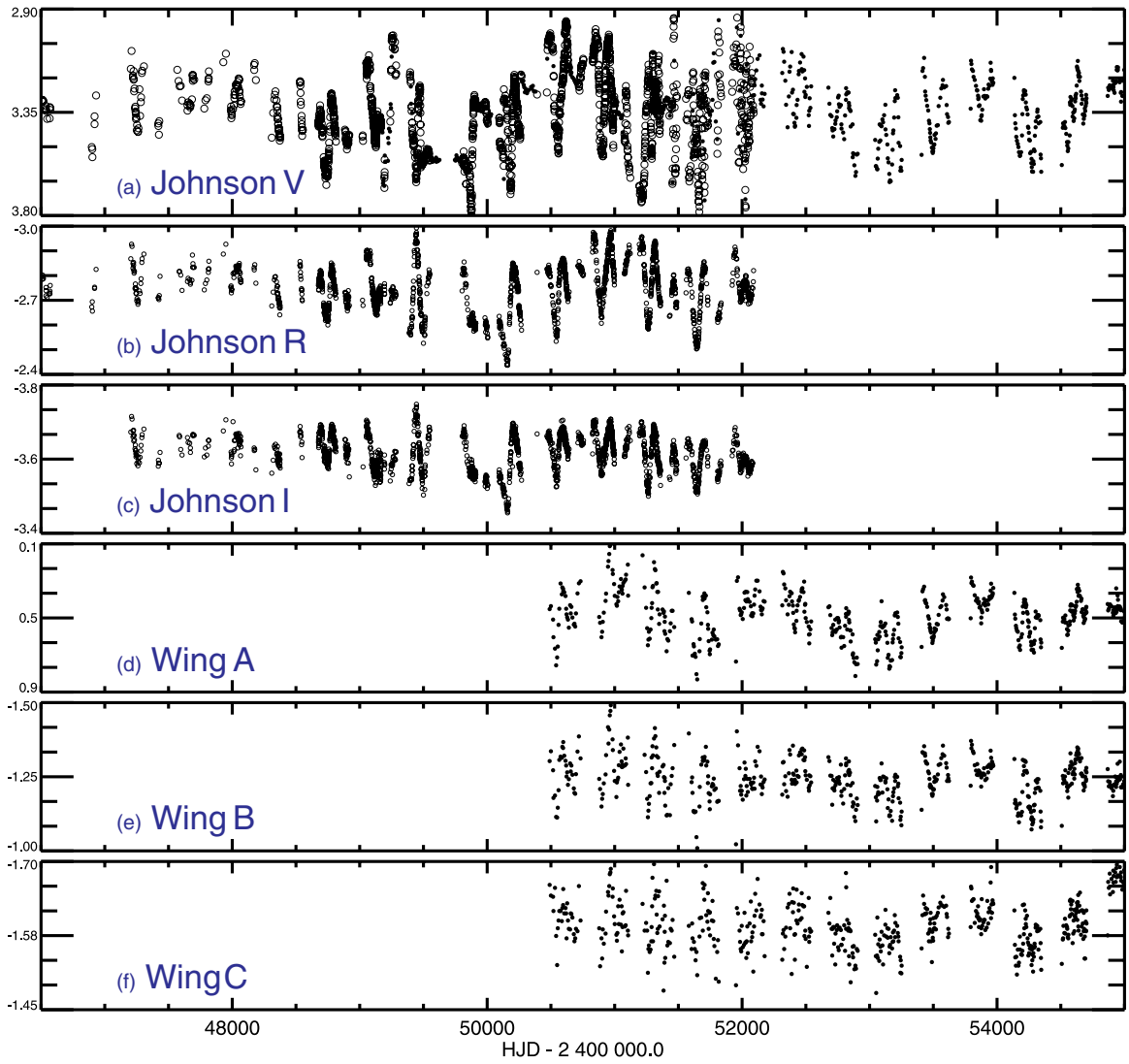

Figure 11. Multi-color, multi-epoch (23 yr) photometry of the α Herculis system. Light curves are presented in increasing central filter wavelengths, and are collected with the Johnson *VRI* and the Wing ABC filters. Empty circles (○) are observations collected at TSU and filled circles (●) are those collected at VU. For more details of the data set, see Section 4 and Table 2. In panel (a), the overlap between the TSU and VU observations are in excellent agreement, and fill out one another's gaps.

(Supplemental data (MRT) for this figure are available in the online journal.)

where x represents the numerical part of the spectral sub-type plus one. For example, to compute the BC_V of an M4.9 star, $x = 5.9$ in Equation (A3). Table 6 lists the calibration stars with their spectral types, V, BC_V, m_{1040}, and BC_C magnitudes, respectively. An average is then taken of all eight bolometric corrections to C to yield the final correction value itself. The bolometric correction to C for each star is given in the last column in Table 6, and the final bolometric correction to C is $BC_C = 1.735 \pm 0.030$. This value is added to the color-corrected C-filter 1040 nm bolometric magnitudes, and these final resulting magnitudes are then used to compute the luminosities in Figure 2 and Table 4.

REFERENCES

Abia, C., Palmerini, S., Busso, M., & Cristallo, S. 2012, A&A, 548, A55
Allen, C. W. (ed.) 1976, Astrophysical Quantities (3rd ed.; London: Athlone)
Angulo, C., Arnould, M., Rayet, M., et al. 1999, NuPhA, 656, 3
Asplund, M., Grevesse, N., Sauval, A. J., & Scott, P. 2009, ARA&A, 47, 481
Baize, P., & Petit, M. 1989, A&AS, 77, 497
Basu, S., Grundahl, F., Stello, D., et al. 2011, ApJL, 729, L10
Basu, S., Verner, G. A., Chaplin, W. J., & Elsworth, Y. 2012, ApJ, 746, 76
Bedding, T. R. 2003, Ap&SS, 284, 61
Benson, J. A., Dyck, H. M., Mason, W. L., et al. 1991, AJ, 102, 2091
Blöcker, T. 1995, A&A, 297, 727
Böhm-Vitense, E. 1958, ZAp, 46, 108
Busso, M., Wasserburg, G. J., Nollett, K. M., & Calandra, A. 2007, ApJ, 671, 802
Cantiello, M., & Langer, N. 2010, A&A, 521, A9
Charbonnel, C., & Lagarde, N. 2010, A&A, 522, A10
Charbonnel, C., & Zahn, J.-P. 2007, A&A, 467, L15
Denissenkov, P. A. 2010, ApJ, 723, 563
Denissenkov, P. A., & Merryfield, W. J. 2011, ApJL, 727, L8
Denissenkov, P. A., & Pinsonneault, M. 2008, ApJ, 684, 626
Deutsch, A. J. 1956, ApJ, 123, 210
Dyck, H. M., Benson, J. A., van Belle, G. T., & Ridgway, S. T. 1996, AJ, 111, 1705
Ekström, S., Georgy, C., Eggenberger, P., et al. 2012, A&A, 537, A146
El Eid, M. F. 1994, A&A, 285, 915
Harris, M. J., & Lambert, D. L. 1984, ApJ, 285, 674
Heger, A., Langer, N., & Woosley, S. E. 2000, ApJ, 528, 368
Heger, A., Woosley, S. E., & Spruit, H. C. 2005, ApJ, 626, 350
Henry, G. W., & Eaton, J. A. (ed.) 1995, in ASP Conf. Ser. 79, Robotic Telescopes: Current Capabilities, Present Developments, and Future Prospects for Automated Astronomy, ed. G. W. Henry & J. A. Eaton (San Francisco, CA: ASP)

Hoffleit, D., & Jaschek, C. (ed.) 1982, The Bright Star Catalogue. Fourth Revised Edition (Containing data compiled through 1979) (New Haven, CT: Yale Univ. Press)
Hoflich, P., Lowe, R. P., Moorhead, J., et al. 1986, MNRAS, 220, 377
Huber, D., Bedding, T. R., Stello, D., et al. 2011, ApJ, 743, 143
Jeffers, H. M., & Vasilevskis, S. 1978, AJ, 83, 411
Karakas, A. I., Campbell, S. W., & Stancliffe, R. J. 2010, ApJ, 713, 374
Keenan, P. C., & McNeil, R. C. 1989, ApJS, 71, 245
Kippenhahn, R., Ruschenplatt, G., & Thomas, H.-C. 1980, A&A, 91, 175
Kiss, L. L., Szabó, G. M., & Bedding, T. R. 2006, MNRAS, 372, 1721
Lacour, S., Thiébaut, E., Perrin, G., et al. 2009, ApJ, 707, 632
Lagarde, N., Decressin, T., Charbonnel, C., et al. 2012, A&A, 543, 108
Langer, N. 2012, ARA&A, 50, 107
Lattanzio, J., & Wood, P. 2004, Asymptotic Giant Branch Stars, ed. J. H. Habing & H. Olofsson (New York: Springer), 23
Lejeune, T., Cuisinier, F., & Buser, R. 1998, A&AS, 130, 65
Levesque, E. M., Massey, P., Olsen, K. A. G., et al. 2005, ApJ, 628, 973
Lockwood, G. W., & Wing, R. F. 1971, ApJ, 169, 63
Maeder, A. (ed.) 2009, Physics, Formation and Evolution of Rotating Stars (Berlin: Springer)
Maeder, A., & Meynet, G. 2001, A&A, 373, 555
Maeder, A., & Meynet, G. 2012, RvMP, 84, 25
Markwardt, C. B. 2009, in ASP Conf. Ser. 411, Astronomical Data Analysis Software and Systems XVIII, ed. D. A. Bohlender, D. Durand, & P. Dowler (San Francisco, CA: ASP), 251
McAlister, H. A., Hartkopf, W. I., Sowell, J. R., Dombrowski, E. G., & Franz, O. G. 1989, AJ, 97, 510
Miglio, A., Chiappini, C., Morel, T., et al. 2013, MNRAS, 429, 423
Moravveji, E., Guinan, E. F., & Sobouti, Y. 2011, in ASP Conf. Ser. 445, Astronomical Society of the Pacific Conference Series, ed. F. Kerschbaum, T. Lebzelter, & R. F. Wing (San Francisco, CA: ASP), 163
Moravveji, E., Guinan, E. F., Wasatonic, R., Sobouti, Y., & Nasiri, S. 2010, Ap&SS, 328, 113
Morel, P., & Thévenin, F. 2002, A&A, 390, 611
Morel, T., Miglio, A., Lagarde, N., et al. 2013, in 40th Liège International Astrophysical Colloquium, Ageing Low Mass Stars: From Red Giants to White Dwarfs, ed. J. Montalbán, A. Noels, & V. Van Grootel (Les Ulis, France: EDP Sciences), 03004
Morgan, W. W., & Keenan, P. C. 1973, ARA&A, 11, 29
Mowlavi, N., Eggenberger, P., Meynet, G., et al. 2012, A&A, 541, A41
Nicholls, C. P., Wood, P. R., Cioni, M.-R. L., & Soszyński, I. 2009, MNRAS, 399, 2063
Paxton, B., Bildsten, L., Dotter, A., et al. 2011, ApJS, 192, 3
Paxton, B., Cantiello, M., Arras, P., et al. 2013, ApJS, 208, 4
Percy, J. R., Wilson, J. B., & Henry, G. W. 2001, PASP, 113, 983
Perrin, G., Ridgway, S. T., Coudé du Foresto, V., et al. 2004, A&A, 418, 675
Perryman, M. A. C., Lindegren, L., Kovalevsky, J., et al. 1997, A&A, 323, L49
Poelarends, A. J. T., Herwig, F., Langer, N., & Heger, A. 2008, ApJ, 675, 614
Rayner, J. T., Cushing, M. C., & Vacca, W. D. 2009, ApJS, 185, 289
Reimers, D. 1977, A&A, 61, 217
Richichi, A., & Percheron, I. 2002, A&A, 386, 492
Smartt, S. J. 2009, ARA&A, 47, 63
Stancliffe, R. J. 2010, MNRAS, 403, 505
Stothers, R. B. 2010, ApJ, 725, 1170
Talon, S., & Charbonnel, C. 2005, A&A, 440, 981
Tassoul, J. 2000, Stellar Rotation, Cambridge Astrophysics Series (Cambridge: Cambridge Univ. Press)
Tatebe, K., Hale, D. D. S., Wishnow, E. H., & Townes, C. H. 2007, ApJL, 658, L103
Thiering, I., & Reimers, D. 1993, A&A, 274, 838
Thompson, R. I., & Johnson, H. L. 1974, ApJ, 193, 147
Thoul, A. A., Bahcall, J. N., & Loeb, A. 1994, ApJ, 421, 828
Thygesen, A. O., Frandsen, S., Bruntt, H., et al. 2012, A&A, 543, A160
Traxler, A., Garaud, P., & Stellmach, S. 2011, ApJL, 728, L29
Unno, W., Osaki, Y., Ando, H., Saio, H., & Shibahashi, H. (ed.) 1989, Nonradial Oscillations of Stars (2nd ed.; Tokyo: Univ. Tokyo Press)
van Leeuwen, F. 2007, A&A, 474, 653
van Loon, J. T. 2006, in ASP Conf. Ser. 353, Stellar Evolution at Low Metallicity: Mass Loss, Explosions, Cosmology, ed. H. J. G. L. M. Lamers, N. Langer, T. Nugis, & K. Annuk (San Francisco, CA: ASP), 211
Weiner, J., Hale, D. D. S., & Townes, C. H. 2003, ApJ, 589, 976
White, N. M., & Wing, R. F. 1978, ApJ, 222, 209
Wing, R. F. 1978, in Spectral Classification and Color Temperature for 280 Bright Stars in the Range K4_M8, Astronomy Dept., Ohio State University
Wing, R. F. 1992, JAVSO, 21, 42
Wood, P. R., Olivier, E. A., & Kawaler, S. D. 2004, ApJ, 604, 800
Woolf, N. J. 1963, Obs, 83, 260